SCIENCE CHINA
Earth Sciences

•RESEARCH PAPER•

March 2021 Vol.64 No.3: 364–376
https://doi.org/10.1007/s11430-020-9668-5

A wave propagation model with the Biot and the fractional viscoelastic mechanisms

Jiaming YANG[1], Dinghui YANG[1*], Hongwei HAN[2], Lingyun QIU[3] & Yuanfeng CHENG[2]

[1] *Department of Mathematical Sciences, Tsinghua University, Beijing 100084, China;*
[2] *Shengli Geophysical Research Institute of SINOPEC, Dongying 257000, China;*
[3] *Yau Mathematical Sciences Center, Tsinghua University, Beijing 100084, China*

Received January 2, 2020; revised July 24, 2020; accepted August 3, 2020; published online October 29, 2020

Abstract Energy loss in porous media containing fluids is typically caused by a variety of dynamic mechanisms. In the Biot theory, energy loss only includes the frictional dissipation between the solid phase and the fluid phase, resulting in underestimation of the dispersion and attenuation of the waves in the low frequency range. To develop a dynamic model that can predict the high dispersion and strong attenuation of waves at the seismic band, we introduce viscoelasticity into the Biot model and use fractional derivatives to describe the viscoelastic mechanism, and finally propose a new wave propagation model. Unlike the Biot model, the proposed model includes the intrinsic dissipation of the solid frame. We investigate the effects of the fractional order parameters on the dispersion and attenuation of the P- and S-waves using several numerical experiments. Furthermore, we use several groups of experimental data from different fluid-saturated rocks to testify the validity of the new model. The results demonstrate that the new model provides more accurate predictions of high dispersion and strong attenuation of different waves in the low frequency range.

Keywords Poroviscoelasticity, Wave propagation, Dispersion and attenuation, Fractional derivative

Citation: Yang J, Yang D, Han H, Qiu L, Cheng Y. 2021. A wave propagation model with the Biot and the fractional viscoelastic mechanisms. Science China Earth Sciences, 64(3): 364–376, https://doi.org/10.1007/s11430-020-9668-5

1. Introduction

Petroleum is one of the most important energy resources for human society, and its exploration has become a research hotspot during the past few decades. Underground geological information is critical in the search for oil reservoirs. One of the most popular methods is the reservoir inversion based on wave propagation models. Therefore, it is of crucial importance to establish an appropriate physical model to simulate the wave propagation in underground porous media. The straightforward wave propagation model is the elastic wave model in isotropic media (Wang et al., 2012). However, the actual media beneath the surface usually consist of the rock frame, fluids and gases (Nie and Yang, 2008). It leads to complex coupling dynamic mechanisms in this multiphase mixture and the inappropriateness of the assumption of the elasticity.

Biot (1956a, 1956b) first established a two-phase wave propagation model that considers the dynamic coupling effects and dissipation mechanisms between the fluid phase and solid phase in porous media. The Biot model laid the foundation for studying linear acoustics of multiphase porous media. Later, Plona (1980) discovered the existence of the slow P-wave in fluid-saturated porous media in experiments, which confirmed the validity of the Biot theory. Subsequently, many scholars have developed a series of effective models based on the Biot theory (White, 1975; Berryman and Thigpen, 1985; Dvorkin and Nur, 1993; Johnson, 2001; Pride et al., 2004; Ba et al., 2008a, 2008b,

* Corresponding author (email: ydh@tsinghua.edu.cn)

2017). However, the energy dissipation in the Biot theory occurs due to the friction caused by the relative movement between the fluid phase and the solid phase at the macroscopic scale. In tight rocks or rocks filled with highly viscous fluids, there is almost no relative macroscopic displacement between the two phases, but experiments still display enormous energy loss and phase velocity dispersion at the seismic band (Pimienta et al., 2017; Yin et al., 2017; Morozov and Deng, 2018), which cannot be interpreted by the Biot theory.

To provide a more appropriate explanation for the above phenomenon, a lot of researchers have made extensive efforts to take other dissipative mechanisms into account. Many experiments have revealed that the heterogeneity due to different pore shapes and distributions can also contribute to wave attenuation (Cheng et al., 2019; Zhang L et al., 2019). Mavko and Nur (1979) first considered the effect of squirt flow mechanism on the waves based on the differences in pore shapes and distributions at microscopic scales. The authors believed that under wave excitation, the fluid in flat fractures of the rock would flow outward in the direction perpendicular to the wave propagation. Afterward, many researchers proposed various models including the squirt-flow mechanism, such as unified models including the squirt-flow and Biot mechanisms (Dvorkin and Nur, 1993; Diallo and Appel, 2000; Parra, 1997; Yang and Zhang, 2000, 2002; Yang et al., 2014), and simplified squirt-flow models using measurable parameters (Gurevich et al., 2010). Generally, the squirt-flow model does provide an adequate interpretation for strong attenuation in low permeability cases (Dvorkin and Nur, 1993; Diallo et al., 2003; Subramaniyan et al., 2015). However, in real subsurface rocks, the velocity dispersion and the strong attenuation predicted by the squirt-flow model mostly occur in the acoustic and ultrasonic bands (Dvorkin et al., 1994, 1995; Gurevich et al., 2010). This result indicates that the squirt-flow model is still lack of accuracy for predicting the dispersion and attenuation, especially in tight rocks in the low frequency range.

In fluid-saturated rocks, the stiffness of the pores is variable due to the heterogeneity of the pores. The fluids inside some stiff pores do not move; thus, we can consider both this part of the fluids and the rock skeleton as a new equivalent solid frame. It is obvious that the new equivalent frame has intrinsic dissipation under wave excitation. Viscoelasticity is widely used to describe this intrinsic dissipation mechanism accurately. The concept of viscoelasticity has existed for a long time. Maxwell (1867), Voigt (1892), Kelvin (1882) and Boltzmann (1878) have successively developed the linear viscoelastic theory. Later, viscoelasticity was included in various poroelastic models to describe wave dispersion and attenuation (Biot, 1962a, 1962b; Cheng et al., 2002; Nie and Yang, 2008; Nie et al., 2010; Xie and Yang, 2018; Zhang B Y et al., 2019), and the concept was also used in wave-field modeling (Arntsen and Carcione, 2001; Du, 2004; Zhang et al., 2018). The inclusion of viscoelasticity in the models provided a more reasonable explanation for the large dispersion and strong attenuation in complex tight rocks.

However, most viscoelastic models are based on the assumption that the medium is linear viscoelastic, which means that its constitutive relationship can be described by a linear combination of several springs and dashpots. However, the dynamic mechanism in porous multiphase media is extremely complicated, and linear viscoelastic models cannot precisely describe the physical properties of the media. A suitable method to improve existing linear viscoelastic models and ensure their applicability to general conditions is using fractional derivatives to replace integral derivatives of the stress and the strain. On the other hand, according to the concept of viscoelasticity, the current status of the stress and strain is determined by their accumulation in the last period, which can be treated as an integral of time in mathematics. This coincides with the definition of the fractional derivative (Samko et al., 1993). Therefore, the viscoelastic properties of the media can be described more precisely by incorporating fractional derivatives into the viscoelastic constitutive relationship (Deng and Morozov, 2018). Furthermore, fractional viscoelastic models can be used to approximate the dispersion and attenuation caused by other mechanisms, such as squirt flow (Carcione and Gurevich, 2011) and patchy saturation (Picotti and Carcione, 2017); thus, fractional viscoelastic models are widely applicable.

In this study, we apply the fractional viscoelastic constitutive relationship to the rock skeleton and establish a new wave propagation model for porous reservoir media based on the Biot theory.

2. Wave propagation model

In this section, we describe the constitutive relationship of 3-D homogeneous isotropic elastic media and generalize it to satisfy the case of fractional viscoelasticity. Then we apply the new constitutive relationship to the solid frame and modify the Biot model to obtain the new wave propagation model.

2.1 Fractional viscoelastic constitutive relationship

The stress-strain relation in 3-D isotropic elastic media is expressed as

$$\sigma_{ij} = \lambda\varepsilon_{kk}\delta_{ij} + 2\mu\varepsilon_{ij}, \tag{1}$$

where σ_{ij} denotes the stress components, ε_{ij} denotes the strain components, and λ and μ are the Lamé constants. Here we use the Einstein summation convention, i.e., $\sigma_{kk}=\sigma_{11}+\sigma_{22}+\sigma_{33}$ and $\varepsilon_{kk}=\varepsilon_{11}+\varepsilon_{22}+\varepsilon_{33}$. We rewrite eq. (1) as

$$\begin{cases}\sigma_{kk}=(3\lambda+2\mu)\varepsilon_{kk}=3K\varepsilon_{kk},\\ S_{ij}=2\mu d_{ij},\end{cases} \tag{2}$$

where K is the bulk modulus, $S_{ij}=\sigma_{ij}-1/3\sigma_{kk}\delta_{ij}$ and $S_{ij}=\sigma_{ij}-1/3\sigma_{kk}\delta_{ij}$ correspond to the deviatoric stress and strain components, respectively. Eq. (2) shows that the bulk stress (σ_{kk}) is proportional to the bulk strain (ε_{kk}) and the deviatoric stress (S_{ij}) is proportional to the deviatoric strain (d_{ij}), which is similar to the 1-D Hooke's law. Therefore, we can separate the stress-strain relationship in 3-D isotropic media into two parts. One is the relationship between the volume change and the bulk stress, and the other is the relationship between the shape change and the shear stress. In real materials, these two stress-strain relationships may be different. For example, the bulk stress of an ideal fluid is proportional to the bulk strain, whereas the deviatoric stress is zero because the fluid cannot bear shear stress; the bulk stress of an incompressible Newtonian fluid is also proportional to the bulk strain, whereas the shear stress is proportional to the change rate of the shear strain. Therefore, real materials exhibit different elastic behaviors under bulk stress and shear stress, and different constitutive relationships can be used to describe the two mechanisms.

Experiments have shown that many subsurface rocks, even tight rocks, display strong attenuation at the seismic band (Batzle et al., 2006; Chapman et al., 2016). Given these facts, we want to introduce the viscoelastic mechanism to describe energy dissipation. For this, following the concept of fractional viscoelastic constitution relationships widely used in material sciences (Pritz, 2003; Konjik et al., 2010), we extend eq. (2) to include the viscoelastic mechanisms for both bulk dilation and shape deformation and obtain the following new viscoelastic constitutive relationship:

$$\begin{cases}\sigma_{kk}+\tau_{\sigma_1}\dfrac{\partial^{\xi_1}}{\partial t^{\xi_1}}\sigma_{kk}=3M_1\left(\varepsilon_{kk}+\tau_{\varepsilon_1}\dfrac{\partial^{\xi_2}}{\partial t^{\xi_2}}\varepsilon_{kk}\right),\\ S_{ij}+\tau_{\sigma_2}\dfrac{\partial^{\beta_1}}{\partial t^{\beta_1}}S_{ij}=2M_2\left(d_{ij}+\tau_{\varepsilon_2}\dfrac{\partial^{\beta_2}}{\partial t^{\beta_2}}d_{ij}\right),\end{cases} \tag{3}$$

where M_1, τ_{ε_1}, τ_{σ_1}, M_2, τ_{ε_2} and τ_{σ_2} are viscoelastic parameters. Specifically, M_1 and M_2 are the static bulk and shear moduli; τ_{ε_1}, τ_{σ_1}, τ_{ε_2} and τ_{σ_2} are the relaxation times. We will discuss how to determine these parameters in the next section. ξ_1, ξ_2, β_1 and β_2 are the orders of the fractional derivatives. The fractional derivative of order α for a function $f(t)$ was provided by Caputo (1976) as follows:

$$D^{\alpha}f(t)=\begin{cases}\dfrac{1}{\Gamma(n-\alpha)}\displaystyle\int_0^t(t-\tau)^{n-\alpha-1}f^{(n)}(\tau)\mathrm{d}\tau, & \alpha\neq n,\\ f^{(n)}(t), & \alpha=n,\end{cases} \tag{4}$$

where $\alpha\in R^{+}$, $n\in N$ and $n-1<\alpha\le n$. $\Gamma(x)$ is the gamma function.

The new fractional viscoelastic constitutive relationship (eq. (3)) can degenerate to an elastic constitutive relationship or Zener's viscoelastic constitutive relationship. Actually, for the elastic case, the strain will respond to a change in stress instantaneously, meaning all relation time parameters (τ_{ε_1}, τ_{σ_1}, τ_{ε_2}, τ_{σ_2}) should be zero. By setting $\tau_{\varepsilon_1}=\tau_{\sigma_1}=\tau_{\varepsilon_2}=\tau_{\sigma_2}=0$, the fractional viscoelastic constitutive relationship (eq. (3)) degenerates to elastic constitutive relationship (eq. (2)). On the other hand, when the fractional order parameters $\xi_1=\xi_2=\beta_1=\beta_2=1$, both constitutive relationships in eq. (3) degenerate to Zener's viscoelastic constitutive relationship (Zener, 1948). Therefore, the new fractional viscoelastic model can be regarded as a generalization of the elastic model and Zener's model. Compared with Zener's model, the orders of the time derivatives in the fractional viscoelastic model can be any positive real number; thus, the proposed model can describe the viscoelastic mechanism more accurately. In other words, this new model can describe the continuous viscoelastic deformation of materials under the stress. Mathematically, the fractional derivative is defined by the integral equation (eq. (4)). By introducing fractional derivatives into viscoelastic relationships, we consider the cumulative stress and strain to establish constitutive relationships. This approach is consistent with the concept of viscoelasticity. From enormous experimental data provided by other researchers (Batzle et al., 2006; Pimienta et al., 2015, 2016, 2017; Spencer and Shine, 2016; Chapman et al., 2016, 2017; Borgomano et al., 2017; Yin et al., 2017; Szewczyk et al., 2018), we select $\xi_1,\xi_2,\beta_1,\beta_2\in(0,2)$. The details will be described in following sections.

We rewrite the viscoelastic constitutive relationship (eq. (3)) in the following convolution form:

$$\begin{cases}\sigma_{kk}=3\psi_1*\dfrac{\partial}{\partial t}\varepsilon_{kk},\\ S_{ij}=2\psi_2*\dfrac{\partial}{\partial t}d_{ij},\end{cases} \tag{5}$$

where ψ_1 and ψ_2 are the relaxation functions. By applying the Fourier transform to eqs. (3) and (5), we obtain

$$\begin{cases}F[\psi_1]=M_1\left(\dfrac{1+(\mathrm{i}\omega)^{\xi_2}\tau_{\varepsilon_1}}{\mathrm{i}\omega+(\mathrm{i}\omega)^{\xi_1+1}\tau_{\sigma_1}}\right),\\ F[\psi_2]=M_2\left(\dfrac{1+(\mathrm{i}\omega)^{\beta_2}\tau_{\varepsilon_2}}{\mathrm{i}\omega+(\mathrm{i}\omega)^{\beta_1+1}\tau_{\sigma_2}}\right),\end{cases} \tag{6}$$

where $F[\cdot]$ represents the Fourier transform. We use the Mittag-Leffler functions to obtain the time-domain expressions of ψ_1 and ψ_2 (Samko et al., 1993). The detailed expressions of ψ_1 and ψ_2 are found in Appendix A (https://link.springer.com). By rewriting eq. (5), we have the following equation:

$$\sigma_{ij}=\left(\psi_1-\frac{2}{3}\psi_2\right)*\frac{\partial}{\partial t}\varepsilon_{kk}\delta_{ij}+2\psi_2*\frac{\partial}{\partial t}\varepsilon_{ij}. \tag{7}$$

Eq. (7) is the proposed new fractional viscoelastic constitutive relationship for a solid frame. In the next subsection, we incorporate eq. (7) into the Biot model to derive a new wave propagation model in fluid-saturated porous media.

2.2 Wave propagation model in fluid-saturated porous media

In the Biot theory, a representative volume element (RVE) of the isotropic fluid-saturated porous media is selected; its governing dynamic equations satisfy the following expressions (Biot, 1956a, 1956b):

$$\begin{cases} \nabla\cdot\boldsymbol{\sigma}=\dfrac{\partial^2}{\partial t^2}(\rho_{11}\mathbf{u}+\rho_{12}\mathbf{U}) \\ \qquad -\dfrac{\eta\phi^2}{\kappa}\dfrac{\partial}{\partial t}(\mathbf{U}-\mathbf{u}), \\ \nabla\cdot(-\phi P\mathbf{I})=\dfrac{\partial^2}{\partial t^2}(\rho_{12}\mathbf{u}+\rho_{22}\mathbf{U}) \\ \qquad +\dfrac{\eta\phi^2}{\kappa}\dfrac{\partial}{\partial t}(\mathbf{U}-\mathbf{u}), \end{cases} \tag{8}$$

where

$$\begin{aligned} \rho_{12}&=-\rho_{\mathrm{a}}, \\ \rho_{11}&=(1-\phi)\rho_{\mathrm{s}}-\rho_{12}, \\ \rho_{22}&=\phi\rho_{\mathrm{f}}-\rho_{12}, \end{aligned} \tag{9}$$

here, ρ_{a} is the additional coupling density, ϕ is the porosity, ρ_{s} is the density of solid grains and ρ_{f} is the fluid density. $\mathbf{u}$ and $\mathbf{U}$ are the displacements of the solid frame and the fluid, respectively; they represent the average displacements of the RVE. $\boldsymbol{\sigma}=(\sigma_{ij})$ represents the stress tensor of the solid frame, P is the fluid pressure and $\mathbf{I}$ is the second-order identity tensor. $\dfrac{\eta\phi^2}{\kappa}\dfrac{\partial}{\partial t}(\mathbf{U}-\mathbf{u})$ on the right side of eq. (8) comes from the dissipation function of the Biot theory, where η is the fluid viscosity and κ is the permeability of the solid frame. In fact, eq. (8) is the motion equation of the RVE.

By substituting the constitutive relationships of the solid frame (Yang and Zhang, 2002) and the fluid pressure (Dvorkin and Nur, 1993)

$$\boldsymbol{\sigma}=\mathbf{A}\boldsymbol{\varepsilon}-(\alpha-\phi)P\mathbf{I}, \tag{10}$$

$$P=-F\frac{\alpha-\phi}{\phi}e-F\gamma, \tag{11}$$

into eq. (8), we obtain the following wave propagation equations:

$$\begin{cases} \nabla\cdot\left(\mathbf{A}\boldsymbol{\varepsilon}+F\dfrac{(\alpha-\phi)^2}{\phi}e\mathbf{I}+F(\alpha-\phi)\gamma\mathbf{I}\right) \\ =\dfrac{\partial^2}{\partial t^2}(\rho_{11}\mathbf{u}+\rho_{12}\mathbf{U})-\dfrac{\eta\phi^2}{\kappa}\dfrac{\partial}{\partial t}(\mathbf{U}-\mathbf{u}), \\ \nabla\cdot(F(\alpha-\phi)e\mathbf{I}+F\phi\gamma\mathbf{I}) \\ =\dfrac{\partial^2}{\partial t^2}(\rho_{12}\mathbf{u}+\rho_{22}\mathbf{U})+\dfrac{\eta\phi^2}{\kappa}\dfrac{\partial}{\partial t}(\mathbf{U}-\mathbf{u}). \end{cases} \tag{12}$$

In eqs. (10)–(12), $\boldsymbol{\varepsilon}=(\varepsilon_{ij})$ and $\mathbf{A}=(a_{ijkl})$ represent the strain tensor and stiffness tensor of the solid frame, respectively. ε_{ij} can be related with $\mathbf{u}$ by using the deformation compatibility equation: $\varepsilon_{ij}=\dfrac{1}{2}\left(\dfrac{\partial u_i}{\partial x_j}+\dfrac{\partial u_j}{\partial x_i}\right)$. The Biot-Willis coefficient α and fluid storage coefficient F are functions of the three bulk moduli (Dvorkin and Nur, 1993):

$$\alpha=1-\frac{K_{\mathrm{m}}}{K_{\mathrm{s}}},\ F=\left(\frac{1}{K_{\mathrm{f}}}+\frac{\alpha-\phi}{\phi K_{\mathrm{s}}}\right)^{-1}, \tag{13}$$

where K_{f}, K_{m} and K_{s} are the bulk moduli of the fluid, the solid frame and the solid grain, respectively. $e=\dfrac{\partial u_1}{\partial x_1}+\dfrac{\partial u_2}{\partial x_2}+\dfrac{\partial u_3}{\partial x_3}$ and $\gamma=\dfrac{\partial U_1}{\partial x_1}+\dfrac{\partial U_2}{\partial x_2}+\dfrac{\partial U_3}{\partial x_3}$ correspond to the dilations of the solid frame and the fluid, respectively. In fact, eq. (12) is equivalent to the wave propagation model in fluid-saturated porous media that was proposed by Biot (1956a).

In the Biot theory, the constitutive relationship is based on the assumption that the solid frame is a perfectly elastic body. However, this is not applicable to real porous materials. Eq. (10) indicates that the elastic properties of the rock frame are contained in the term "$\mathbf{A}\boldsymbol{\varepsilon}$". To describe the viscoelastic mechanism of the rock frame more accurately, we substitute eq. (7) into eq. (10) to obtain the following new constitutive relationship of the solid frame:

$$\begin{aligned} \boldsymbol{\sigma}=&\left(\psi_1-\frac{2}{3}\psi_2\right)*\frac{\partial}{\partial t}e\mathbf{I} \\ &+\psi_2*\frac{\partial}{\partial t}[\nabla\mathbf{u}+(\nabla\mathbf{u})^{\mathrm{T}}]-(\alpha-\phi)P\mathbf{I}. \end{aligned} \tag{14}$$

By substituting eqs. (11) and (14) into eq. (8), we obtain the new wave propagation model including the Biot and fractional viscoelastic mechanisms (simply called the FRVE model) as follows:

$$\begin{cases} \nabla\cdot\left(\left(\psi_1-\dfrac{2}{3}\psi_2\right)*\dfrac{\partial}{\partial t}e\mathbf{I}+\psi_2*\dfrac{\partial}{\partial t}[\nabla\mathbf{u}+(\nabla\mathbf{u})^{\mathrm{T}}]\right. \\ \left.+F\dfrac{(\alpha-\phi)^2}{\phi}e\mathbf{I}+F(\alpha-\phi)\gamma\mathbf{I}\right) \\ =\dfrac{\partial^2}{\partial t^2}(\rho_{11}\mathbf{u}+\rho_{12}\mathbf{U})-\dfrac{\eta\phi^2}{k}\dfrac{\partial}{\partial t}(\mathbf{U}-\mathbf{u}), \\ \nabla\cdot(F(\alpha-\phi)e\mathbf{I}+F\phi\gamma\mathbf{I})= \\ \dfrac{\partial^2}{\partial t^2}(\rho_{12}\mathbf{u}+\rho_{22}\mathbf{U})+\dfrac{\eta\phi^2}{k}\dfrac{\partial}{\partial t}(\mathbf{U}-\mathbf{u}). \end{cases} \tag{15}$$

The main difference between the Biot model and the FRVE model is the first expression in eq. (15), which corresponds to the motion equation of the solid phase. In other words, the FRVE model can degrade to the Biot model by replacing ψ_1 and ψ_2 with the bulk modulus K_{m} and the shear modulus μ_{m} of the frame, respectively. Therefore, the FRVE model is an extension of the Biot model and includes the intrinsic dissipation of the solid frame, whereas the Biot model does not.

In next subsection we will analyze the dispersion and attenuation of different kinds of waves predicted by the new model.

2.3 The phase velocity and attenuation of waves

We conduct a plane-wave analysis using the new model (eq. (15)) to investigate the phase velocity dispersion and energy attenuation of waves. The plane-wave analysis, which is described in Appendix B, allows us to obtain the phase velocities and inverse quality factors of the fast P-wave (V_{p1}, Q_{p1}^{-1}), slow P-wave (V_{p2}, Q_{p2}^{-1}) and the S-wave (V_{s}, Q_{s}^{-1}) as follows:

$$V_{\mathrm{p1,p2}}=\frac{1}{\mathrm{Re}(\sqrt{Y_{\mathrm{p1,p2}}})},\quad Q_{\mathrm{p1,p2}}^{-1}=\frac{2\mathrm{Im}(\sqrt{Y_{\mathrm{p1,p2}}})}{\mathrm{Re}(\sqrt{Y_{\mathrm{p1,p2}}})},\tag{16}$$

$$V_{\mathrm{s}}=\frac{1}{\mathrm{Re}\left(\sqrt{\dfrac{\rho_1+(1-\theta)\rho_2}{M_2^*}}\right)},$$

$$Q_{\mathrm{s}}^{-1}=\frac{2\mathrm{Im}\left(\sqrt{\dfrac{\rho_1+(1-\theta)\rho_2}{M_2^*}}\right)}{\mathrm{Re}\left(\sqrt{\dfrac{\rho_1+(1-\theta)\rho_2}{M_2^*}}\right)},\tag{17}$$

where $Y_{\mathrm{p1,p2}}=-\dfrac{B}{2A}\pm\sqrt{\left(\dfrac{B}{2A}\right)^2-\dfrac{C}{A}}$. The relevant computational formulae are found in Appendix B.

3. Viscoelastic parameters

In the present study, we focus on a reservoir that has not been fractured. Thus the large energy dissipation and negative velocity dispersion induced by scattering in cracked porous media (Winkler, 1983; Jakobsen and Chapman, 2009) are not taken into consideration. On the basis of this assumption, β_1=β_2 and ξ_1=ξ_2; details can be found in Appendix C. For convenience, we let β=β_1=β_2 and ξ=ξ_1=ξ_2 in the next sections. In this case, the new fractional viscoelastic constitutive relationship (eq. (3)) degenerates into the Cole-Cole model (Cole and Cole, 1941). In this relationship, eight viscoelastic parameters (M_1, ω_1, Q_1, M_2, ω_2, Q_2, β, ξ) have to be determined. Following Carcione's work (Carcione, 2007), we define a new set of parameters ω_1, Q_1, ω_2 and Q_2 as

$$\omega_1=(\tau_{\varepsilon_1}\tau_{\sigma_1})^{-\frac{1}{2}},\quad \omega_2=(\tau_{\varepsilon_1}\tau_{\sigma_1})^{-\frac{1}{2}},$$

$$Q_1^{-1}=\frac{1}{2}\left(\sqrt{\frac{\tau_{\varepsilon_1}}{\tau_{\sigma_1}}}-\sqrt{\frac{\tau_{\sigma_1}}{\tau_{\varepsilon_1}}}\right),\tag{18}$$

$$Q_2^{-1}=\frac{1}{2}\left(\sqrt{\frac{\tau_{\varepsilon_2}}{\tau_{\sigma_2}}}-\sqrt{\frac{\tau_{\sigma_2}}{\tau_{\varepsilon_2}}}\right),$$

to replace τ_{ε_1}, τ_{σ_1}, τ_{ε_2} and τ_{σ_2}. The newly defined parameters are directly related to the dispersion and attenuation of the waves. We call ω_1 and ω_2 the reference angular frequencies, and Q_1^{-1} and Q_2^{-1} the reference inverse quality factors.

In fact, all viscoelastic parameters (M_1, ω_1, Q_1, M_2, ω_2, Q_2, β, ξ) are related to macroscopic physical properties. Specifically, M_1, ω_1, Q_1 and ξ describe the viscoelastic mechanism caused by volume dilatation, and M_2, ω_2, Q_2 and β describe the viscoelastic mechanism caused by a shape change. On the basis of eqs. (16) and (17) and following Carcione's method (Carcione, 2007), we provide a theoretical analysis on all viscoelastic parameters below.

M_1 and M_2 are the bulk and shear moduli of the rock frame in the relaxed regime. They describe the stiffness of the frame when there is enough time to return to the equilibrium state, so we have

$$M_1=K_{\mathrm{m}},\ M_2=\mu_{\mathrm{m}},\tag{19}$$

where K_{m} and μ_{m} are the bulk and shear moduli of the dry frame. Furthermore, M_1 and M_2 are closely related with the low-frequency limit of the phase velocities of fast P- and S-waves. The two reference frequencies ω_1 and ω_2 are associated with the frequencies where the attenuation peaks of the fast P-wave and S-wave appear. The values of Q_1^{-1} and Q_2^{-1}, are closely related to the attenuation peak values and the phase velocity dispersion magnitudes of the fast P-wave and S-wave. ξ and β describe the transition of the fast P-wave and S-wave between the relaxed regime and the unrelaxed regime.

We provide two approaches to determine the values of the viscoelastic parameters ω_1, ω_2, Q_1^{-1}, Q_2^{-1}, ξ and β. The first method consists of inverting these viscoelastic parameters by fitting a few phase velocity or attenuation data measured at different frequencies (Yang et al., 2014; Liu et al., 2018). The second method is based on stress oscillation experiments (Pimienta et al., 2015, 2016). Specifically, we provide an oscillating confining pressure on the sample and measure the variation of strain. By analyzing the attenuation behaviors of the sample, we can calculate these viscoelastic parameters.

4. Numerical examples

In this section, we investigate the effects of ξ and β on the dispersion and attenuation of fast P- and S-waves. Here we suppose that the rock sample is water-saturated. The physical properties and viscoelastic parameters of the sample are listed in Table 1. In first numerical experiment, we choose ξ=1 and different values of β to observe the changes in the phase velocities and inverse quality factors of the fast P- and S-waves. Similarly, we choose β=1 and change the values of ξ in the second numerical example. The computational re-

sults are displayed in Figure 1.

Figure 1a–1d correspond to the case of ξ=1 and show the effects of different values of β on the phase velocity dispersion and attenuation of the fast P- and S-waves. Figure 1a and 1c show the phase velocities of the S-wave and fast P-wave, respectively. Obviously, there is a large dispersion between 10 and 1000 Hz and the dispersion transition becomes narrower with increasing β. However, the results calculated by the Biot model show no visible dispersion in the low frequency range. Meanwhile, all high-frequency limits of phase velocities computed by the FRVE model are the same for the three cases of β=0.8, 1 and 1.2, which are larger than that computed by the Biot model. One interesting phenomenon is that the phase velocities of the S-wave and the fast P-wave decrease slightly from 1 to 10 Hz for β=1.2. According to investigations of wave scattering in poroelastic media (Hudson, 1981; Blair, 1990; Morochnik and Bardet, 1996), we believe that this dispersion is similar to the Rayleigh scattering associated with randomly distributed and oriented cracks in porous media. This result indicates that we can apply the fractional viscoelastic model (β=1.2) to characterize the attenuation induced by wave scattering. In Figure 1b and 1d, all three cases (β=0.8, 1, and 1.2) of the FRVE model have an attenuation peak in the low frequency range. As β increases, the attenuation peak shifts towards lower frequencies and its value increases. The numerical results show that the fractional-order parameter β has significant effects on the dispersion and attenuation of the two waves in the low frequency range.

Figure 1e–1h show the changes in the wave attenuation and dispersion as ξ increases for β=1. Figure 1g and 1h show the phase velocities and inverse quality factors of the fast P-wave, respectively. Similar to the results in Figure 1c and 1d, a large velocity dispersion and strong attenuation is observed due to the viscoelastic mechanism. In addition, as ξ increases, the transition range of the velocity dispersion of the fast P-wave becomes narrower, the attenuation peak of the fast P-wave shifts towards a lower frequency, and its value decreases. However, as shown in Figure 1e and 1f, the phase velocities and inverse quality factors of the S-wave are the same for the three cases (ξ=0.8, 1 and 1.2), indicating that the dispersion and attenuation of the S-wave are independent of the parameter ξ. Hence, we conclude that ξ only affects the dispersion and attenuation of the fast P-wave.

5. Applications

5.1 Unconventional reservoir examples

In this subsection, we use the dispersion data of two water-saturated tight rock cores to testify the validity of the FRVE model. The rock cores are provided by the Exploration and Development Research Institute of PetroChina Changqing Oilfield Company, and the data are obtianed by the Key Laboratory of Geophysics of the China National Petroleum Corporation. The two cores used in this experiment are drilled from the Sulige gas field. One is a sandstone sample (A11), and the other is a dolomite sample (C12). Both cores have low permeabilities less than 0.3 mD and low porosities less than 10%. The cores are saturated by water and the dispersion data are measured in the frequency band of 1–1171 Hz. The physical properties are listed in Table 2.

Table 1 Physical properties and viscoelastic parameters of the fluid-saturated sample

Name	Values
Fluid density ρ_f (kg m^{-3})	1000
Fluid viscosity η (Pa•s)	0.001
Fluid bulk modulus K_f (GPa)	2
Porosity ϕ (%)	10
Permeability κ (mD)	1
Solid-phase density ρ_s (kg m^{-3})	2650
Solid frame bulk modulus K_m (GPa)	16
Solid material bulk modulus K_s (GPa)	38
Solid frame shear modulus μ_m (GPa)	8
Solid-fluid coupling density ρ_a (kg m^{-3})	420
Reference angular frequency ω_1	100
Reference angular frequency ω_2	100
Reference quality factor Q_1	20
Reference quality factor Q_2	20

We calculate the phase velocity dispersions of the S-wave and fast P-wave using the Biot model and the FRVE model, and compare the numerical results with the measured data. The results are displayed in Figure 2. The fast P- and S-waves show high velocity dispersion in the frequency range of 1–100 Hz. However, there is no obvious dispersion of the phase velocities computed by the Biot model in the low frequency range. Actually, following the definition of the characteristic frequency used in the Biot theory (Biot, 1956a)

$$f_c = \frac{\eta\phi}{2\pi\kappa\rho_f}, \tag{20}$$

which represents the frequency corresponding to the attenuation peak induced by the Biot's dissipation mechanism, we obtain the characteristic frequencies 5.34×10^7 Hz and 1.15×10^8 Hz for core A11 and core C12, respectively. The result implies that the velocity dispersion and attenuation predicted by the Biot model mainly occur in the frequency range of 10^7–10^9 Hz for the two cores. Therefore, the Biot model cannot explain the high velocity dispersion in the seismic frequency range. In contrast, the phase velocities computed by the FRVE model provide a good fit to the measured data (Figure 2), indicating that the viscoelastic

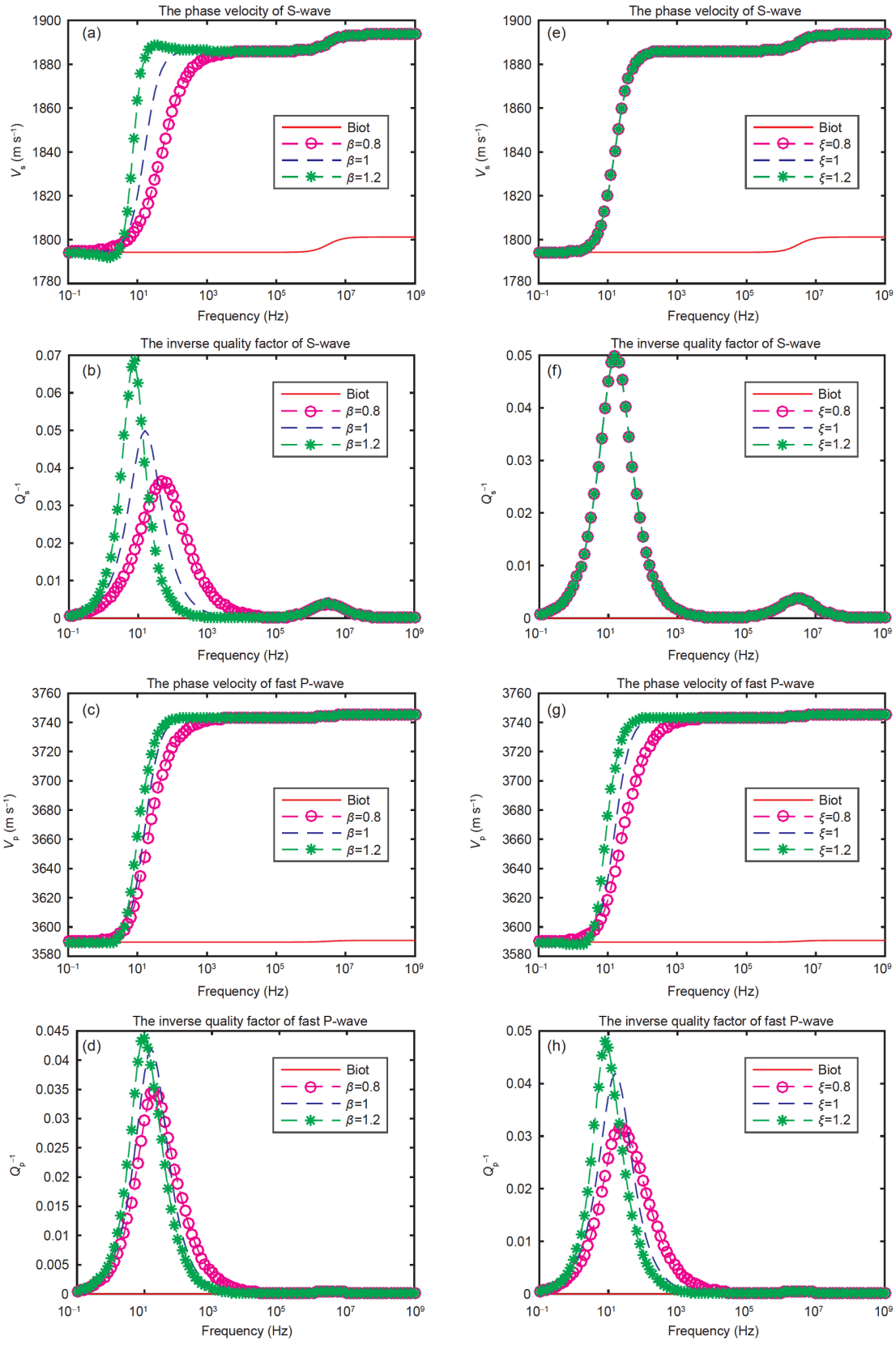

Figure 1 Effects of fractional order parameters (ξ and β) on the dispersion and attenuation of waves for the first test model. The physical properties and viscoelastic parameters of the sample are listed in Table 1. (a) and (e) show the phase velocities of the S-wave; (b) and (f) show the inverse quality factors of the S-wave; (c) and (g) show the phase velocities of the fast P-wave; (d) and (h) show the inverse quality factors of the fast P-wave. In (a)–(d), ξ=1; in (e)–(h), β=1.

Table 2 Physical properties of the water-saturated rock cores from Changqing Oilfield

Physical properties	A11	C12
Fluid density ρ_f (kg m^{-3})	1000	1000
Fluid viscosity η (Pa•s)	0.001	0.001
Fluid bulk modulus K_f (GPa)	2.18	2.18
Porosity ϕ (%)	9.39	8.55
Permeability κ (mD)	0.280	0.118
Solid-phase density ρ_s (kg m^{-3})	2664.2	2894.9
Solid frame bulk modulus K_m (GPa)	16.53	32.68
Solid material bulk modulus K_s (GPa)	38.00	89.65
Solid frame shear modulus μ_m (GPa)	21.55	26.83
Solid-fluid coupling density ρ_a (kg m^{-3})	420	420

mechanism is the primary reason for the energy loss in tight rocks at low frequencies.

Based on the above numerical results, we have some physical explanations below. As we mentioned in the Introduction Section, the energy loss predicted by the Biot model is caused by the macroscopic relative movement between the solid phase and the fluid phase. However, due to the low permeability and low porosity for the tight cores, the fluid movement inside the pores may not be a Poiseuille flow, even there is no macroscopic relative movement between the rock frame and the pore fluids. Hence, the Biot dissipation in the cores is negligible. On the other hand, since the solid part accounts for more than 90% of the cores, its intrinsic dissipation cannot be neglected. Due to the poor connectivity in tight cores, some pores are sealed, and the fluids inside such pores move in conjunction with the rock skeleton. In other pores, a portion of the fluid is constrained by electrostatic forces along the pore walls. Although there is no macroscopic relative movement between the rock skeleton and these fluids, the elastic properties of the saturated cores may be affected under a pressure gradient. Therefore,

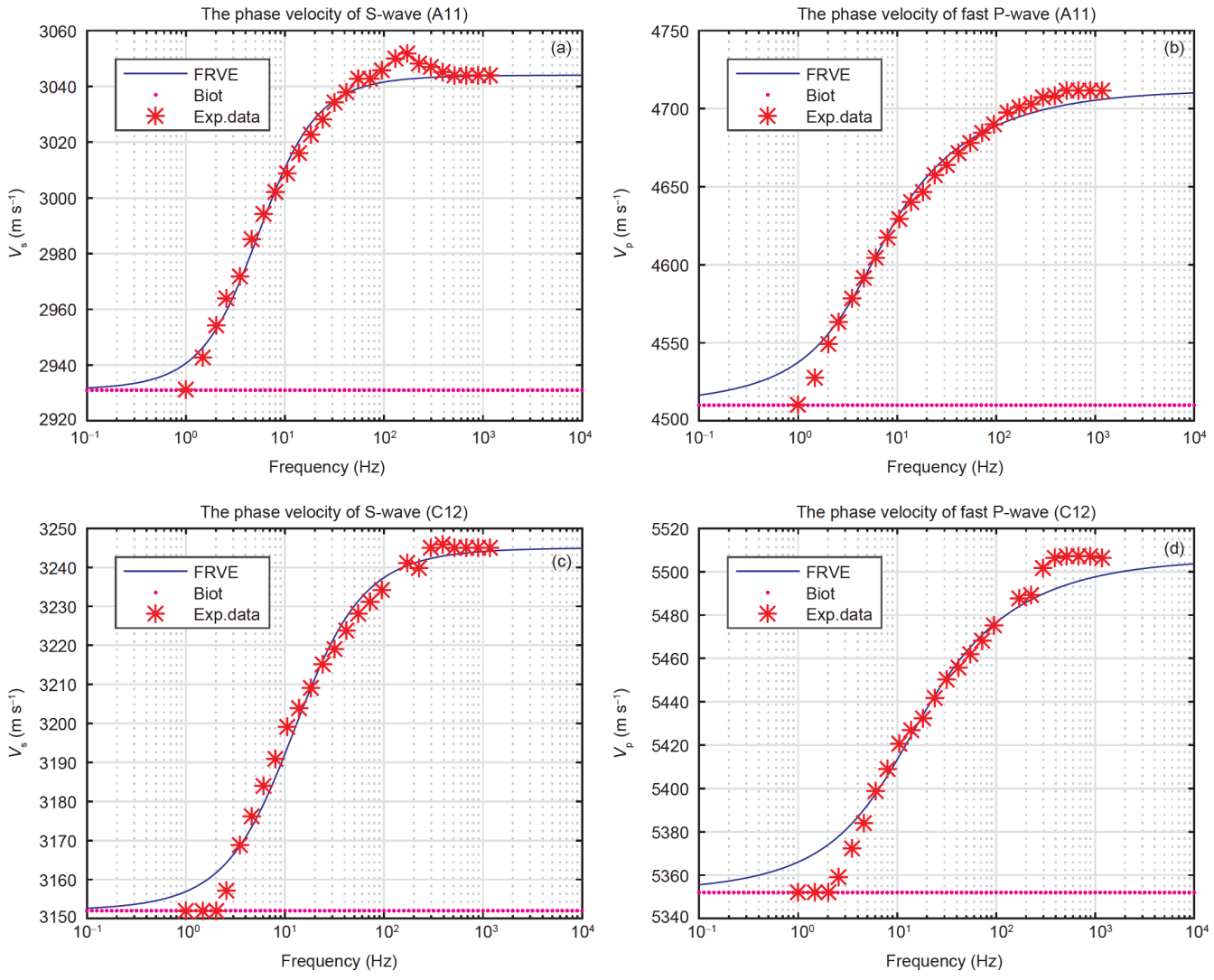

Figure 2 Comparison of the experimental data and the numerical results for unconventional reservoirs. The physical properties of the two samples are listed in Table 2. (a) and (b) show the results for the core A11; (c) and (d) show the results for the core C12. Discrete stars represent the experimental data.

we treat these fluids and the rock skeleton as a new solid "frame". Obviously, the new frame is viscoelastic and its inner friction contributes to the energy loss, which we believe is the primary reason for the phase velocity dispersion at the seismic band.

From the comparisons of numerical results and analyses stated above, we conclude that the FRVE model provides better predictions of the dispersion and attenuation of the waves in unconventional reservoirs than the Biot model.

5.2 Conventional reservoir examples

In this subsection, we will demonstrate that the FRVE model is also suitable for conventional reservoirs. Here we use several groups of experimental data provided by Spencer and Shine (2016). The two rock cores (labeled as LF176 and LF177) used in this experiment are Lower Miocene sandstones collected from the deepwater Gulf of Mexico, and the dominant grains of the rocks are quartz. These samples are visually homogeneous in a thin-section photomicrograph; thus, they can be considered as isotropic media. The two samples have high porosity (20.9% and 19.7%) and high permeability (115 and 58 mD) and are saturated with different Cannon hydrocarbon viscosity standard fluids labeled as N100 and N35, respectively. The experiments conducted by Spencer and Shine (2016) were performed at room temperature under a confining pressure of 17.24 MPa (2500 psi) and a pore pressure of 3.45 MPa (500 psi). The physical properties of the standard fluids and rock cores are listed in Tables 3 and 4, respectively.

The dispersion and attenuation of Young's modulus E and Poisson's ratio ν of the saturated rock sample were measured in a wide frequency band of 0.2–205 Hz by Spencer and Shine (2016). Transformations of E and ν are required to obtain the dispersion and attenuation data of the P-wave and S-wave.

Based upon the elastic wave propagation theory, the phase velocities of the P-wave and S-wave can be expressed by E and ν as

$$V_{\mathrm{p}}=\sqrt{\frac{E(1-\nu)}{\rho(1+\nu)(1-2\nu)}},\ V_{\mathrm{s}}=\sqrt{\frac{E}{2\rho(1+\nu)}}, \tag{21}$$

where $\rho=\phi\rho_{\mathrm{f}}+(1-\phi)\rho_{\mathrm{s}}$ represents the density of the saturated rock sample. In Appendix D, we describe the inverse quality factors of the P- and S-waves that were obtained through a series of operations. Furthermore, we can obtain all viscoelastic parameters (ω_1, Q_1, ω_2, Q_2, β, ξ) included in the FRVE model by fitting the phase velocity data of the P- and S-waves. In this experiment, we get β=0.63 and ξ=0.50 for the sample LF176, and β=0.47 and ξ=0.36 for the sample LF177. Based on the obtained fractional-order parameters and physical properties listed in Tables 3 and 4, we compute the theoretical phase velocities and inverse quality factors of the fast P- and S-waves by using the FRVE model. The results (solid line) are shown in Figures 3 and 4. To compare with other models, we also exhibit the theoretical results computed by the Biot model (dotted line) and the linear viscoelastic model (dashed line) in Figures 3 and 4. Here, the linear viscoelastic model (simply called the LV model) is the special case of the FRVE model with ξ=β=1.

Table 3 Physical properties of the two Cannon hydrocarbon viscosity standard fluids

Physical properties	N100	N35
Fluid density ρ_{f} (kg m^{-3})	875.6	867.3
Fluid viscosity η (Pa•s)	0.301	0.077
Fluid bulk modulus K_{f} (GPa)	2.136	2.015

Table 4 Physical properties of the two Lower Miocene sandstones collected from the deepwater Gulf of Mexico

Physical properties	LF176	LF177
Porosity ϕ (%)	20.9	19.7
Permeability κ (mD)	115	58
Solid-phase density ρ_{s} (kg m^{-3})	2650	2650
Solid frame bulk modulus K_{m} (GPa)	9.04	10.21
Solid material bulk modulus K_{s} (GPa)	44.24	44.24
Solid frame shear modulus μ_{m} (GPa)	9.81	10.40
Solid-fluid coupling density ρ_{a} (kg m^{-3})	420	420

In Figures 3a, 3c, 4a and 4c, there is an obvious dispersion for the fast P-wave (2.6–4.3%) and S-wave (2.1–2.9%) at the seismic band. However, the phase velocities calculated by the Biot model remain constant in the low frequency range, and the values are far away from the experimental data. Similar to the last subsection, we calculate the Biot characteristic frequencies of LF176 (9.94×10^7 Hz) and LF177 (5.10×10^8 Hz). The results show that the Biot dissipation occurs in the ultrasonic band around 10^7–10^8 Hz for these samples LF176 and LF177. Therefore, the attenuation and dispersion at the seismic band are not caused by the Biot dissipation mechanism. In contrast, the phase velocities computed by the FRVE model and the LV model match well with the experimental data, unlike the Biot model. Thus, we believe that the viscoelastic mechanism is the primary reason for the large dispersion and strong attenuation in this experiment. Additionally, Figures 3 and 4 show that the new model fits the experimental data better than the LV model.

In Figures 3b, 3d, 4b and 4d, both the fast P-wave and the S-wave exhibit strong attenuation in the frequency range of 0.2–205 Hz. Specifically, the measured inverse quality factor increases as the frequency grows. However, there is no visible attenuation in the inverse quality factor curves cal-

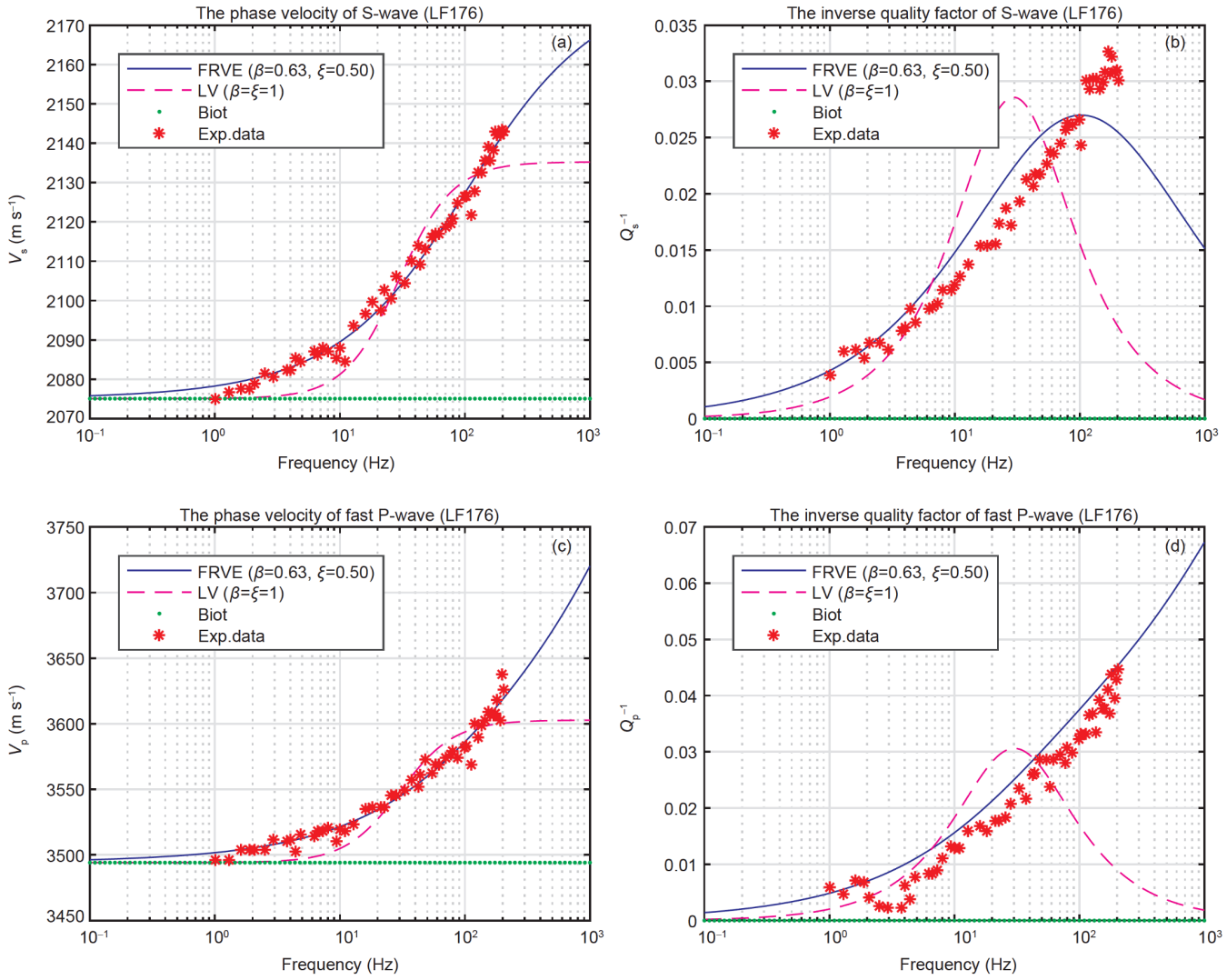

Figure 3 Comparison of the measured data and theoretical results computed by three models. The sample is LF176 saturated with N100. (a) Phase velocities of the S-wave; (b) inverse quality factors of the S-wave; (c) phase velocities of the fast P-wave; (d) inverse quality factors of the fast P-wave.

culated by the Biot model, indicating the failure of the attenuation prediction. In contrast, the numerical results computed by the FRVE model and the LV model display strong attenuation and are much closer to the experimental data. Moreover, in Figures 3d, 4b and 4d, wave attenuations predicted by the LV model have an attenuation peak around 10–100 Hz, whereas the results computed by the FRVE model show no attenuation peaks below 10^3 Hz and are more consistent with the experimental data than those computed by the LV model. Based on the comparisons, we conclude that the FRVE model performs better than the existing viscoelastic model and the Biot model for the prediction of wave dispersion and attenuation in conventional reservoirs.

6. Discussion and conclusions

In this study, we suggest a generalized fractional viscoelastic constitutive relationship by replacing the integer time derivatives in the Zener viscoelastic model with fractional derivatives. Based on the framework of the Biot theory, we apply this fractional viscoelastic constitutive relationship to the solid frame of fluid-saturated porous rocks and propose a new poroviscoelastic wave propagation model including the fractional viscoelastic mechanism, simply called the FRVE model. This new FRVE model is a generalization of the linear poroviscoelastic model. In other words, when the fractional-order parameters β and ξ are integers, the FRVE model degrades to the conventional poroviscoelastic model.

We investigate the validity and accuracy of the new model for predicting the phase velocities and attenuations of the fast P- and S-waves using experimental data. The numerical results show that the FRVE model provides more accurate predictions when compared with the famous Biot model and linear viscoelastic model for unconventional and conventional reservoirs. Moreover, the numerical results also de-

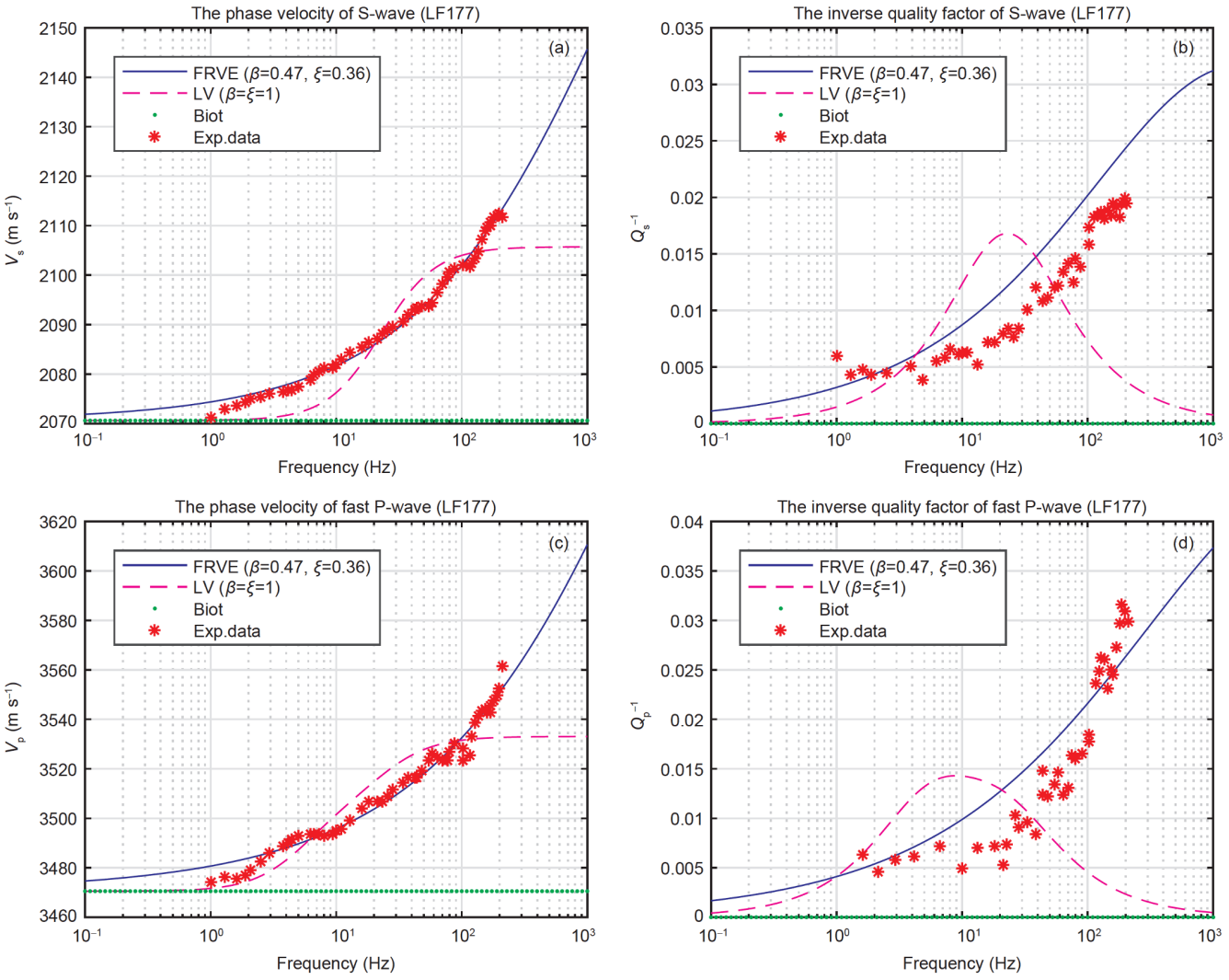

Figure 4 Comparison of the measured data and theoretical results computed by three models. The sample is LF177 saturated with N35. (a) Phase velocities of the S-wave; (b) inverse quality factors of the S-wave; (c) phase velocities of the fast P-wave; (d) inverse quality factors of the fast P-wave.

monstrate that the fractional order parameter β affects the dispersion and attenuation of both the fast P- and S-waves, whereas another parameter ξ only affects the fast P-wave.

Due to the generality and the continuity of the fractional order, the FREV model can accurately describe wave propagation in complex reservoirs and is suitable for different porous media, such as fluid-saturated tight dolomites and sandstones with high permeability. On the basis of the time-domain FREV model, we can implement the temporal-spatial forward modeling of waves and reservoir parameter inversion in unconventional and conventional oil/gas reservoirs to provide valuable information for petroleum prospecting. It is expected that the new FREV model will have wide applications in complex reservoirs.

Acknowledgements *The authors thank the Exploration and Development Research Institute of PetroChina Changqing Oilfield Company for providing the experimental data. This work was supported by the National Natural Science Foundation of China (Grant Nos. 91730306 and 41390452) and the Shengli Oilfield Company (Grant No. 30200020-18-ZC0613-0030).*

References

Arntsen B, Carcione J M. 2001. Numerical simulation of the Biot slow wave in water-saturated Nivelsteiner Sandstone. Geophysics, 66: 890–896

Ba J, Cao H, Yao F, Nie J, Yang H. 2008a. Double-porosity rock model and squirt flow in the laboratory frequency band. Appl Geophys, 5: 261–276

Ba J, Nie J X, Cao H, Yang H Z. 2008b. Mesoscopic fluid flow simulation in double-porosity rocks. Geophys Res Lett, 35: L04303

Ba J, Xu W, Fu L Y, Carcione J M, Zhang L. 2017. Rock anelasticity due to patchy saturation and fabric heterogeneity: A double double-porosity model of wave propagation. J Geophys Res-Solid Earth, 122: 1949–1976

Batzle M L, Han D H, Hofmann R. 2006. Fluid mobility and frequency-dependent seismic velocity—Direct measurements. Geophysics, 71: N1–N9

Berryman J G, Thigpen L. 1985. Effective constants for wave propagation through partially saturated porous media. Appl Phys Lett, 46: 722–724

Biot M A. 1956a. Theory of propagation of elastic waves in a fluid-satu-

rated porous solid. I. Low-frequency range. J Acoust Soc Am, 28: 168–178
Biot M A. 1956b. Theory of propagation of elastic waves in a fluid-saturated porous solid. II. Higher frequency range. J Acoust Soc Am, 28: 179–191
Biot M A. 1962a. Generalized theory of acoustic propagation in porous dissipative media. J Acoust Soc Am, 34: 1254–1264
Biot M A. 1962b. Mechanics of deformation and acoustic propagation in porous media. J Appl Phys, 33: 1482–1498
Blair D P. 1990. A direct comparison between vibrational resonance and pulse transmission data for assessment of seismic attenuation in rock. Geophysics, 55: 51–60
Boltzmann L. 1878. Zur theorie der elastischen nachwirkung. Ann Phys Chem, 241: 430–432
Borgomano J V M, Pimienta L, Fortin J, Guéguen Y. 2017. Dispersion and attenuation measurements of the elastic moduli of a dual-porosity limestone. J Geophys Res-Solid Earth, 122: 2690–2711
Caputo M. 1976. Vibrations of an infinite plate with a frequency independent *Q*. J Acoust Soc Am, 60: 634–639
Carcione J M. 2007. Wave Fields in Real Media: Wave Propagation in Anisotropic, Anelastic, Porous and Electromagnetic Media. 2nd ed. Amsterdam: Elsevier
Carcione J M, Gurevich B. 2011. Differential form and numerical implementation of Biot's poroelasticity equations with squirt dissipation. Geophysics, 76: N55–N64
Chapman S, Quintal B, Tisato N, Holliger K. 2017. Frequency scaling of seismic attenuation in rocks saturated with two fluid phases. Geophys J Int, 208: 221–225
Chapman S, Tisato N, Quintal B, Holliger K. 2016. Seismic attenuation in partially saturated berea sandstone submitted to a range of confining pressures. J Geophys Res-Solid Earth, 121: 1664–1676
Cheng W, Ba J, Fu L Y, Lebedev M. 2019. Wave-velocity dispersion and rock microstructure. J Pet Sci Eng, 183: 106466
Cheng Y F, Yang D H, Yang H Z. 2002. Biot/squirt model in viscoelastic porous media. Chin Phys Lett, 19: 445–448
Cole K S, Cole R H. 1941. Dispersion and absorption in dielectrics i. Alternating current characteristics. J Chem Phys, 9: 341–351
Deng W, Morozov I B. 2018. Mechanical interpretation and generalization of the cole-cole model in viscoelasticity. Geophysics, 83: MR345–MR352
Diallo M S, Appel E. 2000. Acoustic wave propagation in saturated porous media: Reformulation of the biot/squirt flow theory. J Appl Geophys, 44: 313–325
Diallo M S, Prasad M, Appel E. 2003. Comparison between experimental results and theoretical predictions for p-wave velocity and attenuation at ultrasonic frequency. Wave Motion, 37: 1–16
Du Q Z. 2004. Wavefield forward modeling with the pseudo-spectral method in viscoelastic and azimuthally anisotropic media (in Chinese). Acta Phys Sin, 53: 4428–4434
Dvorkin J, Mavko G, Nur A. 1995. Squirt flow in fully saturated rocks. Geophysics, 60: 97–107
Dvorkin J, Nolen-Hoeksema R, Nur A. 1994. The squirt-flow mechanism: Macroscopic description. Geophysics, 59: 428–438
Dvorkin J, Nur A. 1993. Dynamic poroelasticity: A unified model with the squirt and the Biot mechanisms. Geophysics, 58: 524–533
Gurevich B, Makarynska D, de Paula O B, Pervukhina M. 2010. A simple model for squirt-flow dispersion and attenuation in fluid-saturated granular rocks. Geophysics, 75: N109–N120
Hudson J A. 1981. Wave speeds and attenuation of elastic waves in material containing cracks. Geophys J Int, 64: 133–150
Jakobsen M, Chapman M. 2009. Unified theory of global flow and squirt flow in cracked porous media. Geophysics, 74: WA65–WA76
Johnson D L. 2001. Theory of frequency dependent acoustics in patchy-saturated porous media. J Acoust Soc Am, 110: 682–694
Kelvin W T B. 1882. Mathematical and Physical Papers: Vol 3: Elasticity, Heat, Electro-Magnetism. Cambridge: Cambridge University Press
Konjik S, Oparnica L, Zorica D. 2010. Waves in fractional zener type viscoelastic media. J Math Anal Appl, 365: 259–268
Liu X, Greenhalgh S, Zhou B, Greenhalgh M. 2018. Effective biot theory and its generalization to poroviscoelastic models. Geophys J Int, 212: 1255–1273
Mavko G M, Nur A. 1979. Wave attenuation in partially saturated rocks. Geophysics, 44: 161–178
Maxwell J C. 1867. On the dynamical theory of gases. Philos Trans R Soc London, 157: 49–88
Morochnik V, Bardet J P. 1996. Viscoelastic approximation of poroelastic media for wave scattering problems. Soil Dyn Earthq Eng, 15: 337–346
Morozov I B, Deng W. 2018. Inversion for biot-consistent material properties in subresonant oscillation experiments with fluid-saturated porous rock. Geophysics, 83: MR67–MR79
Nie J X, Yang D H. 2008. Viscoelastic BISQ model for low-permeability sandstone with clay. Chin Phys Lett, 25: 3079–3082
Nie J X, Yang D H, Ba J. 2010. Velocity dispersion and attenuation of waves in low-porosity-permeability anisotropic viscoelastic media with clay (in Chinese). Chin J Geophys, 53: 385–392
Parra J O. 1997. The transversely isotropic poroelastic wave equation including the biot and the squirt mechanisms: Theory and application. Geophysics, 62: 309–318
Picotti S, Carcione J M. 2017. Numerical simulation of wave-induced fluid flow seismic attenuation based on the cole-cole model. J Acoust Soc Am, 142: 134–145
Pimienta L, Borgomano J V M, Fortin J, Guéguen Y. 2017. Elastic dispersion and attenuation in fully saturated sandstones: Role of mineral content, porosity, and pressures. J Geophys Res-Solid Earth, 122: 9950–9965
Pimienta L, Fortin J, Guéguen Y. 2015. Experimental study of Young's modulus dispersion and attenuation in fully saturated sandstones. Geophysics, 80: L57–L72
Pimienta L, Fortin J, Guéguen Y. 2016. Effect of fluids and frequencies on Poisson's ratio of sandstone samples. Geophysics, 81: D183–D195
Plona T J. 1980. Observation of a second bulk compressional wave in a porous medium at ultrasonic frequencies. Appl Phys Lett, 36: 259–261
Pride S R, Berryman J G, Harris J M. 2004. Seismic attenuation due to wave-induced flow. J Geophys Res, 109: B01201
Pritz T. 2003. Five-parameter fractional derivative model for polymeric damping materials. J Sound Vib, 265: 935–952
Samko S G, Kilbas A A, Marichev O I. 1993. Fractional Integrals and Derivatives: Theory and Applications. New York: CRC
Spencer J W, Shine J. 2016. Seismic wave attenuation and modulus dispersion in sandstones. Geophysics, 81: D211–D231
Subramaniyan S, Quintal B, Madonna C, Saenger E H. 2015. Laboratory-based seismic attenuation in fontainebleau sandstone: Evidence of squirt flow. J Geophys Res-Solid Earth, 120: 7526–7535
Szewczyk D, Bauer A, Holt R M. 2018. Stress-dependent elastic properties of shales—Laboratory experiments at seismic and ultrasonic frequencies. Geophys J Int, 212: 189–210
Voigt W. 1892. Ueber innere reibung fester körper, insbesondere der metalle. Ann Phys Chem, 283: 671–693
Wang M X, Yang D H, Song G J. 2012. Semi-analytical solutions and numerical simulations of 2d sh wave equation (in Chinese). Chin J Geophys, 55: 914–924
White J E. 1975. Computed seismic speeds and attenuation in rocks with partial gas saturation. Geophysics, 40: 224–232
Winkler K W. 1983. Frequency dependent ultrasonic properties of high-porosity sandstones. J Geophys Res, 88: 9493–9499
Xie P Y, Yang D H. 2018. Seismic wave propagation model in near-surface strong-attenuation media (in Chinese). Chin J Geophys, 61: 917–925
Yang D H, Zhang Z J. 2000. Effects of the biot and the squirt-flow coupling interaction on anisotropic elastic waves. Chin Sci Bull, 45: 2130–2138
Yang D H, Zhang Z J. 2002. Poroelastic wave equation including the biot/squirt mechanism and the solid/fluid coupling anisotropy. Wave Motion, 35: 223–245
Yang L, Yang D H, Nie J X. 2014. Wave dispersion and attenuation in

viscoelastic isotropic media containing multiphase flow and its application. Sci China-Phys Mech Astron, 57: 1068–1077
Yin H J, Zhao J G, Tang G Y, Zhao L M, Ma X Y, Wang S X. 2017. Pressure and fluid effect on frequency-dependent elastic moduli in fully saturated tight sandstone. J Geophys Res-Solid Earth, 122: 8925–8942
Zener C. 1948. Elasticity and Anelasticity of Metals. Chicago: University of Chicago Press. 544–568
Zhang B Y, Yang D H, Cheng Y F, Zhang Y Y. 2019. A unified poroviscoelastic model with mesoscopic and microscopic heterogeneities. Sci Bull, 64: 1246–1254
Zhang J B, Yang D H, He X J, Ma X. 2018. Discontinuous galerkin method for solving wave equations in two-phase and viscoelastic media (in Chinese). Chin J Geophys, 61: 926–937
Zhang L, Ba J, Fu L Y, Carcione J M, Cao C H. 2019. Estimation of pore microstructure by using the static and dynamic moduli. Int J Rock Mech Min Sci, 113: 24–30

(Responsible editor: Ling CHEN)